Biophysical Chemistry 5 (1976) 301–318

THE FLEXIBILITY OF LOW MOLECULAR WEIGHT DOUBLE-STRANDED DNA AS A FUNCTION OF LENGTH.

II. Light scattering measurements and the estimation of persistence lengths from light scattering, sedimentation and viscosity‡

Jamie E. GODFREY* and Henryk EISENBERG

Department of Polymer Research, The Weizmann Institute of Science, Rehovot, Israel, and Department of Biology, The Johns Hopkins University, Baltimore, Maryland 21218, USA

Received 4 December 1975
Revised manuscript 1 April 1976

In the preceding paper are described the isolation and physical characterization of seven narrowly disperse fractions of calf thymus DNA in the molecular weight range 0.3 to 1.3 × 10^6 daltons. Herein, we have determined by light scattering the molecular weights and root mean square radii of these fractions in a solvent comprising 0.2 M NaCl, 2 mM EDTA, 2mM Na-PO_4, pH 7. Measurements were made in a modified Wippler–Scheibling photometer to a 20° lower limit of scattering angle on solutions rendered virtually dust-free by procedures described. The optical anisotropies of the DNA fractions were measured permitting the experimental molecular weights and root mean square radii to be corrected to their true values. From these values, with appropriate polydispersity corrections, we calculate a Kratky–Porod persistence length, a, of 54.0 ± 5.6 nm which is invariant over the molecular weight range examined. From the sedimentation coefficients (preceding paper) and the theory of Yamakawa and Fujii, we calculate a to be 66 nm, a value found to apply equally well to several DNA samples of various origins whose sedimentation rates are known in the molecular weight range from about 4 × 10^4 to 10^8 daltons. Similarly, from the intrinsic viscosities and the theory of Yamakawa and Fujii, we calculate a to be 59 nm, which again adequately applies to a number of DNA samples whose viscosities have been measured by other workers in the molecular weight range 3 × 10^5 to 10^8 daltons. The Flory–Mandelkern parameter, β, was found to vary with molecular weight in the manner predicted by the theory of Yamakawa and Fujii. The average value of a from the three sets of measurements is 60 ± 6 nm, which we believe applies to double-stranded DNA molecules, independent of chain length, over the whole range of molecular weights for which reliable data exist.

1. Introduction

The accompanying paper [1] describes the isolation and physical characterization of seven fractions from sonically fragmented calf thymus DNA. They were found to be narrowly disperse with weights ranging from 0.3 to 1.3 × 10^6 daltons, and their sedimentation rates and intrinsic viscosities varied linearly, and highly precisely, with molecular weight in double-logarithmic plots. The present work reports results from elastic light scattering measurements on these fractions which are then used in conjunction with the molecular weight and polydispersity data of the first paper to estimate the Kratky–Porod persistency length, a, [2] characterizing the DNA fragments of each fraction.

Because estimates of persistence lengths from particle contour lengths and root mean square radii (or radii of gyration) are very sensitive to errors in these parameters [3,4] – particularly in the case of short chain molecules – optical anisotropy corrections were applied [5,6]. For the lowest molecular weight fractions,

‡ This work was supported in part by Project No. 06–05901 granted to the Weizmann Institute of Science under the Special International Research Program of the National Institutes of Health, U.S. Public Health Service.

* Recipient during the course of this research of a Postdoctoral Fellowship from the Muscular Dystrophy Associations of America, Inc., and a Weizmann Senior Fellowship.

these corrections to the values determined for the Z-average root mean square radius ($\langle R^2 \rangle \equiv R_{gz}$, in subsequent notation) were quite significant. Moreover, since the optical anisotropy ratios were found to vary inversely with chain length and the fractions were polydisperse, the anisotropy corrections to the persistence length calculations were somewhat complex. To better estimate the limiting angular dependence of the scattering intensities (which defines R_{gz}), the light scattering photometer used in these experiments (Fica model 4200), was modified to allow intensity readings down to scattering angle $\theta = 19°$; in addition, techniques were developed to produce virtually dust-free sample solutions to ensure reliable measurements in the low θ range.

Persistence lengths are also estimated from the velocity sedimentation and viscosity measurements. For this purpose, we have relied on the recent papers of Yamakawa and Fujii on the translational properties [7] and intrinsic viscosity [8] of wormlike chains; these authors critically discuss earlier work and dwell on the difficulties deriving from the limitations of the hydrodynamic treatments or the lack of a complete distribution function for the configuration of the wormlike coil. Their treatment is in reasonable agreement with some of the earlier contributions (cf. Hearst and Stockmayer [9]); however, it has the advantage that, as a result of considerable advances in computer technologies, experimental verification over a wide range of variables is possible by use of extensive tables of calculated results, provided by the authors. The treatment of Yamakawa and Fujii is particularly attractive for DNA, as it is based on the properties of a flexible rod of well defined dimensions (an excellent representation of the DNA molecule) rather than the earlier representations of touching beads.

2. Materials and methods

Chemicals were reagent grade and water was doubly glass distilled.

2.1. Light scattering

Measurements were made in a Wippler–Scheibling light scattering photometer [10] (Fica, Paris, model no. 4200) which had been modified earlier to accomodate filters and polarizers in the scattered beam. For the present study two additional modifications were made: the bracket holding the glass stray light absorber in the toluene bath was trimmed to the width of the absorber, and an auxiliary absorber was mounted next to the detector collimating slit on the side of lower angular setting; these alterations allowed scattering intensities to be measured at angles, θ, as low at 19° to the incident beam, an extension of 11° below the instrument's normal θ range. Cuvettes were optical grade borate–silicate glass cylinders (0.9 mm wall thickness and 30 mm in diameter) with flat bottoms and ground glass stoppered filling ports; the minimum volume required for measurements was about 8 ml.

The basic components of the instrument were aligned following the procedure recommended by the manufacturer. Polarizers in the incident and scattered beams (required for the present study) were carefully aligned using the partially vertically polarized light emitted by the incident beam slit when it was closed down to its minimum setting as the primary polarization axis standard. Benzene which was first passed through a silica gel and aluminum oxide Woelm column [11], to remove possible traces of fluorescent impurities, and then distilled directly into a dust-free cuvette was used as the primary scattering standard. The values of Coumou [12] for the absolute Rayleigh ratios of benzene at the two incident wavelengths were used in all calculations (i.e., 4.56×10^{-5} and 1.58×10^{-5} cm^{-1} at 436 and 546 nm, respectively). The benzene standard was also used to test the symmetry of the scattered beam intensities around $\theta_{90°}$ after alignment of the optical system; the measured intensities between $\theta_{150°}$ and $\theta_{30°}$ agreed with values furnished by the manufacturer. To evaluate the accuracy of the scattering intensities recorded in the angular region below $\theta_{30°}$ (allowed by the modifications described above), the benzene standard and very dilute solutions of fluorescein in water were analyzed by the procedure of Cohen and Eisenberg [11]. It was found that accurate readings were possible down to $\theta_{19°}$; moreover, the same analysis yielded depolarization ratios (ρ_u) of benzene of 0.429 and 0.427 at 436 and 546 nm, respectively, in close agreement with published values [11–13].

Solutions of DNA dissolved in solvent B (see section 2 of the accompanying paper [1]) and solvent blanks were measured at 15 or more scattering angles between $\theta_{20°}$ and $\theta_{150°}$ at two incident beam wavelength, 436 and 546 nm, isolated by the incident beam filters supplied

with the instrument. For most series of measurements, vertical Polaroid polarizers were placed in both the incident and scattered beams. For measurements intended to evaluate the electrical anisotropy of the DNA fractions, a horizontal polarizer was used in place of the vertical element in the scattered beam. At angles below 30°, it was often found necessary to average the four values read at 90° rotational intervals of the sample cell; the variations observed in these readings were due in large part to slight deviations from the vertical in cell orientation. A glass rod furnished by the manufacturer was calibrated against the benzene sample and used as the working scattering standard throughout the measurements.

Because the filtration procedure followed in producing dust-free DNA solutions (see below) may have selectively removed small amounts of the larger fragments, light scattering measurements on the fractions were carried out first; all experiments described in the accompanying paper [1] were then subsequently done on the highest concentration light scattering sample of each fraction.

2.2. Preparation of dust-free solutions

Accurate measurements of scattering intensities at low values of θ were particularly important to these studies. It was essential, therefore, to exclude contaminating dust from the sample solutions since at low angles the scattering intensities of large particles are markedly enhanced. Solution contamination has plagued light scattering measurements on biopolymers dissolved in aqueous media for many years. Because of the success enjoyed in our laboratory in eliminating this problem, a detailed description of the techniques developed would perhaps be welcomed. We have found that clean solutions depend primarily on preparing clean cuvettes initially; i.e., the principle source of particulate contamination is the cuvette and not the solution introduced. The latter can easily be made virtually dust-free by filtration.

We produce dust-free cuvettes as follows: Cells are first soaked overnight in dichromate cleaning solution. After repeated rinsing in distilled water, they are immersed in 1 M NaOH for 10 minutes and again repeatedly rinsed with distilled water; the alkaline treatment was found to greatly enhance the hydrophilic properties of the cell walls. Each cell is then attached directly to an all-glass still designed to distill-over dust-free water. This still is fitted with a 100 cm × 2.5 cm reflux column filled with Pyrex rings; potassium permanganate is added to the distilling flask to oxidize any organic matter. The distillate elutes from a glass capillary fitted with a hood (fashioned from the lower half of a 5 ml disposable syringe barrel) which prevents air-borne dust from entering the cuvette during filling (fig. 1a). After 3–4 rinses, the cell is capped with a square of aluminum foil and the disymmetry of the water measured in the light scattering photometer at $\theta_{30°}$ and $\theta_{150°}$. The operation is repeated until the disymmetry ratio is < 1.15. The cell is emptied of water as before but the last few drops are allowed to cover the bottom of a "drying cup" (shown in fig. 1b). The cell is immediately inverted on the cup and both cup and cell transferred to a clean drying oven at 150°C. The seal between cup rim and cell allows water vapor to escape but prevents dust from entering. The 0.5 ml of water in the cup does not evaporate until after the cell is completely dry; it thus acts as a trap for any dust in the system in a way similar to the oil reservoir in an oil bath air cleaner used on automobile carburators. When the water in the cup has also dried, the unit is removed from the oven, intact, and allowed to cool to room temperature under a bell jar. Finally, the cell is sealed as before with a square of aluminum foil and is now ready for the introduction of clean solvent.

Two liters of stock solvent were made up relatively dust-free by first filtering a concentrated solution of

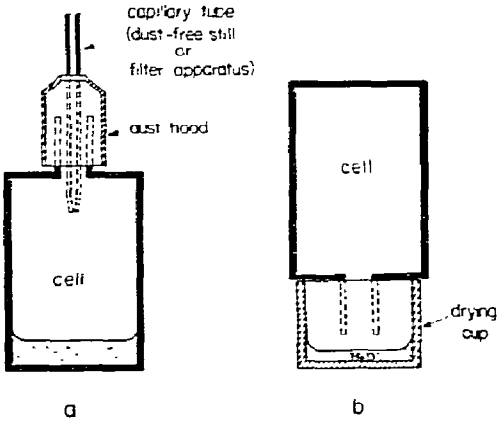

Fig. 1. Technique for producing dust-free solutions (explanations in section 2).

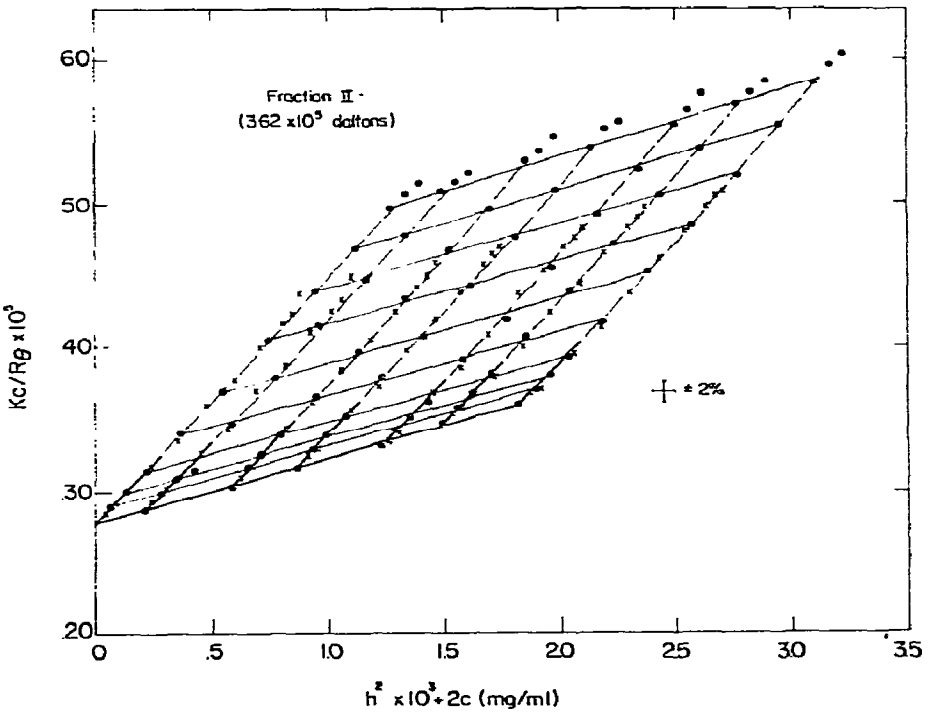

Fig. 2a. Zimm plot of data from fraction II. Abscissa is in units of h^2 to allow intensities recorded at both incident beam wavelengths to be co-plotted. (•) at 436 nm; (×) at 546 nm. Solid lines: data points included in linear least squares extrapolations to zero angle and infinite dilution used in determining M_w^* and R_{gz}^{2*}. Data points at several values of θ below 45° omitted for clarity. Measurements at 25°C.

the solvent components through a 50 nm Millipore disc under vacuum into a clean volumetric flask and then filling to volume directly from the still described above. This preliminary cleaning extended the effective lifetime of the filter discs used in the cuvette filling operations that followed. Solvent was introduced into clean light scattering cells in 8–12 ml volumes through a 0.22 μm Millipore disc supported on a filtering assembly which had been modified as follows: (1) the sintered glass disc which normally supports the central area of the filter was removed allowing the filter to be supported only at its periphery; (2) the delivery stem was replaced by a capillary tube of approximately 12 cm in length and drawn to a narrow tip. After dichromate cleaning, the unit was rinsed with distilled water and, while still wet, fitted with the filter disc. 20–30 ml of dust-free water were then passed through by gravity followed by a similar volume of solvent to flush residual contaminants from the capillary and to rid the filter of loose cellulose debris (it was necessary that the capillary be filled with liquid to produce an adequate flow rate). Prior to cell filling, a hood similar to that used on the still effluent tube was fitted to the capillary stem about 2 cm from its tip. With solvent passing through the unit, a clean cell was quickly placed beneath the hood (between drops) as shown in fig. 1a. Eluent drops fell freely to the cell bottom; the ground glass surface of the filling port was not allowed to be wetted. After the desired volume of solvent had dripped into the cell, it was removed and immediately covered with a square of aluminum foil. Solvent volumes — required for estimating the amount of DNA solution to be added — were determined from cell weight differences before and after filling. The disymmetry of the solvent was then measured in the light scattering photometer. When the above procedure was followed, it

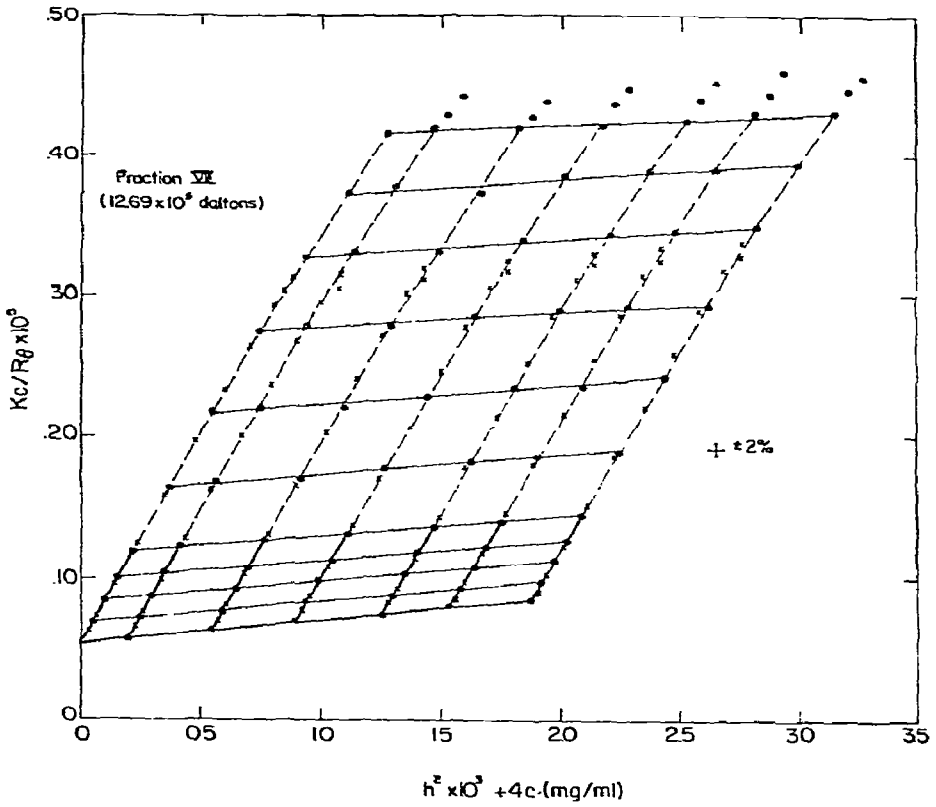

Fig. 2b. Zimm plot of data from Fraction VII. See legend fig. 2a.

was found that over 90% of the solvents produced were dust-free, with $I_{30°}/I_{150°} < 1.02$. No special precautions were found to be necessary, e.g., dust-free environments, gloves, etc.[‡]

In a separate operation (usually the following day), concentrated DNA solution was added to the clean solvents in varying amounts using the same filtering procedure described above. After the square of aluminum foil was added, a secure, air-tight seal was made by wrapping the fill port stem with ca. 10 cm of Teflon pipe thread tape. The stoppers supplied with the cells were not used in order to avoid the possibility of minute fragments of glass from the ground glass surfaces falling into the solutions when the stoppers were seated. The solutions were swirled for 30 seconds or more to insure complete mixing and generally stored overnight to allow microscopic air bubbles, which may have been incorporated into the solutions during the filling process, to dissipate. Rough estimates of the DNA concentrations were made from weight differences of the cell before and after introduction of the DNA and the solvent volumes calculated earlier. Precise determination of concentrations were made after the scattering measurements from OD_{259} values of weighed dilutions in the manner described previously [1].

2.3. Determination of $(\partial n/\partial c)_\mu$

The specific refractive index increasement, $(\partial n/\partial c)_\mu$, for sonicated DNA dissolved in solvent B (see section 2 of the accompanying paper [1]) was measured in the Beckman Model E analytical ultracentrifuge by the

‡ One of us (J.G.) discovered that he could smoke a cigar throughout the procedure with no ill effect on the quality of the solutions produced.

synthetic boundary method [14]. Sonicated DNA, not further fractionated, at a concentration of 0.9 mg/ml in solvent B was centrifuged at 20000 rpm in a fixed angle rotor for one hour. The upper four-fifths of the supernatant was carefully decanted and further centrifuged at 40000 rpm for 24 hours. The pellet was redissolved in solvent B to a concentration of 4 mg/ml and exhaustively dialyzed against this solvent at room temperature. DNA solution and dialysate were introduced in appropriate volumes into a 1.2 cm double-sector cell fitted with an alluminum-filled epon capillary-type synthetic boundary centerpiece. Dialysate overlay was effected at 4000–5000 rpm, and Rayleigh interference patterns of the spreading boundary were photographed at 2–4 minute intervals with one of two filters alternately in place above the mercury light source; these filters were narrow band pass monochromatic incident beam filters from a Fica 50 (Fica, Paris) light scattering photometer with maximum transmissions at 546 and 436 nm. Blank correction runs were made in the usual way.

Fringe deviations were recorded on the Nikon microcomparator described earlier [1] at 500 μ intervals along the x axis and the values graphed after numerical corrections for the cell blank. An average y value for each plateau region was determined (they were quite flat for about 10 minutes after overlayering), and their difference used to calculate the fractional fringe shift through the boundary. The fractional fringe shift values were extrapolated back to t_0 in order to correct for boundary sedimentation; this correction, however, was found to be insignificant for interferograms recorded during the first 10 minutes after overlay was effected. DNA concentrations were determined from the 259 nm absorbancies. $(\partial n/\partial c)_\mu$ at 546 and 436 nm were found to be 0.160 and 0.166 ml/g, respectively.

The light scattering data was analyzed with the aid of a Fortran IV computer program designed by Dori Cwikel of our laboratory; a Fortran IV computer program for estimating persistence lengths from light scattering measurements and particle length distributions was written by Allen Kakala of the Johns Hopkins University Computer Center.

3. Basic equations for light scattering, the Kratky–Porod worm-like coil, sedimentation and viscosity

3.1. Light scattering

The light scattering data were analyzed by the two familiar equations [4,10]:

$$(Kc/\Delta R)_{\theta=0} = M_w^{*-1} + 2A_2c + \dots, \quad (1)$$

$$(Kc/\Delta R)_{c=0} = [M_w^* P^*(\theta)]^{-1}$$

$$= M_w^{*-1}[1 + \tfrac{1}{3}h^2 R_{gz}^{2*} + \dots], \quad (2)$$

where

$$K = (\partial n/\partial c)_\mu^2 \, 2\pi^2 n_0^2/(\lambda_0^4 N_A),$$

$$h = (4\pi n_0/\lambda_0)\sin\theta/2,$$

and

$$\Delta R = (\Delta I/I_B) V_v \, R_B (V_v/U_u)_B \, (n_0/n_B)^2.$$

A_2 is the second virial coefficient; c is the concentration in g/ml; N_A is Avogadro's number; λ_0 is the incident wavelength, in vacuo; n_0 is the solvent refractive index; $(\partial n/\partial c)_\mu$ is the refractive index increment at constant chemical potential of diffusible components (water and salt) [15]; ΔI is the measured scattering intensity of the solution corrected for solvent at any scattering angle; I_B is the scattering intensity of the benzene standard at $\theta_{90}°$; the subscript V_v refers to measurements with vertical polarizers placed in both the incident and scattered beams; $(n_0/n_B)^2$ is the beam geometry correction factor applicable to the Sofica instrument required to compensate for the difference in refractive index between solvent and benzene; R_B is the Rayleigh ratio of benzene evaluated under conditions of unpolarized light (U_u); and $(V_v/U_u)_B$ is the ratio of the scattering intensities of benzene under the two indicated light polarization conditions at $\theta_{90}°$. This last factor is required to correct R_B to conditions of V_v; from the Krishnan relations [16], (V_v/U_u) is found to be equivalent to $(2-\rho_u)/(1+\rho_u)$, where ρ_u is the depolarization ratio (H_u/V_u) at $\theta_{90}°$. Using the values for ρ_u reported in the previous section, $(V_v/U_u)_B$ is 1.099 and 1.102 at 436 and 546 nm, respectively.

Measurements were made with vertical polarizers

placed in both the incident and scattered beams in order to evaluate the contributions to the scattering intensities from the optical anisotropies of the DNA fragments. Eqs. (1) and (2) yield an apparent weight average molecular weight (M_w^*) and an apparent Z-average mean square radius (R_{gz}^{2*}). For rod-like particles under conditions of V_v, these parameters are correctable (for $\delta \ll 1$) to their true values by [5,6]:

$$M_w = M_w^*/(1+\delta^2), \tag{3}$$

$$R_{gz}^2 = R_{gz}^{2*}\left(\frac{35 - 28\delta + 20\delta^2}{7(5+4\delta^2)}\right)^{-1}. \tag{4}$$

δ is the optical anisotropy ratio defined as:

$$\delta = (\gamma_1 - \gamma_2)/3\Delta\gamma, \tag{5}$$

where γ_1 and γ_2 are the two polarizabilities of the solute, and $\Delta\gamma$ is the excess polarizability of the solute over the solvent $[\Delta\gamma = (n_0/\pi)(\partial n/\partial c)(M/N)]$. δ^2 can be evaluated from the relationship,

$$\delta^2 = \left(\frac{5\rho_v}{3-4\rho_v}\right)_{\theta=0}, \tag{6}$$

where ρ_v is the depolarization ratio of the solute under conditions of vertically polarized incident light (H_v/V_v). The sign of δ is evaluated from the scattering angle where the scattering intensity measured under conditions of H_h is minimized:

$$\theta_{min} < \pi/2, \quad \delta > 0; \qquad \theta_{min} > \pi/2, \quad \delta < 0. \tag{7}$$

For DNA, Weil et al. [6] have established that δ is negative.

3.2. The Kratky–Porod worm-like coil

The mean square end-to-end distance of a continuously bending stiff coil can be expressed in terms of its contour length, L, and a stiffness parameter, the persistence length, a [2,4].

The latter is defined as the average extension of an infinitely long chain on the axis of its initial propagation; a increases with chain stiffness and will equal infinity for a rigid rod. Benoit and Doty [17] have related a and L to the root mean square radius which allows persistence lengths to be estimated from light scattering measurements:

$$R_g^2 = 2aL\left(\frac{1}{6} - \frac{a}{2L} + \frac{a^2}{L^2} - \frac{a^3}{L^3}(1 - e^{-L/a})\right). \tag{8}$$

For DNA, L is obtained from the molecular weight and the known mass per unit length in salt solutions, 1950 daltons/nm, the value calculated for the B structure [18,19].

Since the root mean square radius measured by light scattering is the Z-average, and the molecular weights measured by light scattering and sedimentation equilibrium are weight averages (for the latter method, the weight average is the most reliable moment obtainable), corrections for polydispersity must be applied in order to obtain accurate estimates of persistence lengths from eq. (8). These corrections will be described in the next section.

3.3. Sedimentation and viscosity

The sedimentation coefficient s, in Svedberg units, for a linear polymer is expressed (in the formalism of Yamakawa and Fujii [7]) by

$$s = [\lambda M(1 - \phi'\rho)/N_A \Xi] \times 10^{20}, \tag{9}$$

where $1/2\lambda$ is the persistence length a (in nm units), ϕ' is an apparent volume appropriate for multicomponent systems [15], ρ is the solvent density, and Ξ is the frictional coefficient, in units of λ^{-1}. The frictional coefficient Ξ_∞ of an infinitely long and flexible chain is given by

$$\Xi_\infty = 3\pi\eta_0 L^{1/2}/A_1. \tag{10}$$

Ξ is determined by the theory from chain dimensions and λ; Yamakawa and Fujii define a function:

$$\Gamma_2(L, d) \equiv 3 \log (\Xi_\infty/\Xi),$$

where

$$L = \lambda(M/M_L) \tag{11}$$

is the reduced contour length (in units of λ^{-1}), d is the reduced diameter of the macromolecular chain, and M_L is the mass per unit length (daltons/nm). A_1 is a constant:

$$A_1 = \tfrac{4}{3}(6/\pi)^{1/2} = 1.8426. \tag{12}$$

It is now possible to rewrite eq. (9) in the form

$$\log s = \log [(1 - \phi' \rho)/\eta_0] + \log M_L + \log (10^{20} A_1/3\pi N_A) + \tfrac{1}{3}\Gamma_2 + \tfrac{1}{2}\log L. \quad (13)$$

For the interpretation of the intrinsic viscosity, $[\eta]$, we write, again following Yamakawa and Fujii [10],

$$[\eta] = (\Phi/10^{21})(L^{3/2}/\lambda^3 M), \quad (14)$$

where $[\eta]$ is the unreduced intrinsic viscosity, in dl/g, Φ is a function of L and d and is derived from the theory, and the other quantities have been defined before. The value $\Phi_\infty = 2.87 \times 10^{21}$ is well known in hydrodynamic theory of polymeric chains.

Yamakawa and Fujii define a function:

$$\Gamma_1(L, d) \equiv \log (\Phi_\infty/\Phi) \quad (15)$$

in analogy to Γ_2 defined in sedimentation. Some elementary transformation of eq. (14) now yields

$$\tfrac{2}{3}\log (M_L^{3/2} [\eta]/2.87 M^{1/2}) = \log \lambda^{-1} - \tfrac{2}{3}\Gamma_1. \quad (16)$$

Finally, we may combine eqs. (13) and (16), eliminate λ, and obtain the Flory–Mandelkern equation,

$$10^{-13} s[\eta]^{1/3} \eta_0 N_A/(1 - \phi' \rho) M^{2/3} = \beta, \quad (17)$$

where

$$\beta(L, d) = 10^{(\Gamma_2 - \Gamma_1)/3} A_1 \phi_\infty^{1/3}/3\pi. \quad (18)$$

4. Experimental results and calculations

4.1. Light scattering measurements

Values of $Kc/\Delta R$ were plotted by the double extrapolation method of Zimm [20]. Only the six (or for some fractions, seven) values recorded between $\theta_{20}°$ and $\theta_{45}°$ were included in the extrapolations to infinite dilution and $\theta_0°$; all extrapolations were by linear least squares fit. Fig. 2 shows Zimm plots obtained for Fractions II and VII (25°C); data points at both incident wavelengths are included, normalized to the function h^2 (eq. (2)). The reduced zero angle plots of all seven fractions are seen in fig. 3. The line for each fraction is defined by the average values for the slopes and intercepts obtained from the least squares analyses of the data at the two incident wavelengths. The corresponding reduced infinite dilution plots are shown in fig. 4; again, the lines represent the averages of the data at the two incident wavelengths.

Apparent weight average molecular weights and apparent Z-average mean square radii (both uncorrected for the effects of optical anisotropy) were calculated from these data (eqs. (1) and (2)) and are listed in table 1. It should be noted that the two least squares extrapolation procedures – to infinite dilution and to $\theta_0°$ – necessarily yield identical ordinate intercept values $(1/M_w^*)$. The nonideal behavior of the DNA fragments is reflected in the positive slopes seen in fig. 3. The second virial coefficients calculated from the slopes (eq. (1)) are found in table 2 of the accompanying paper [1], where they can be compared with the values obtained from sedimentation equilibrium experiments.

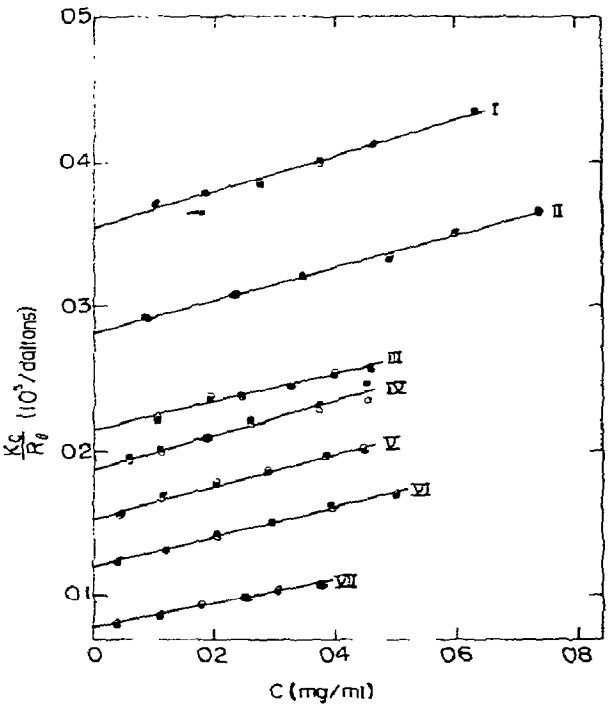

Fig. 3. Zero angle extrapolates for fractions I–VII. (○) at 436 nm; (●) at 546 nm. Extrapolations are by linear least squares fit. Measurements made at 25°C.

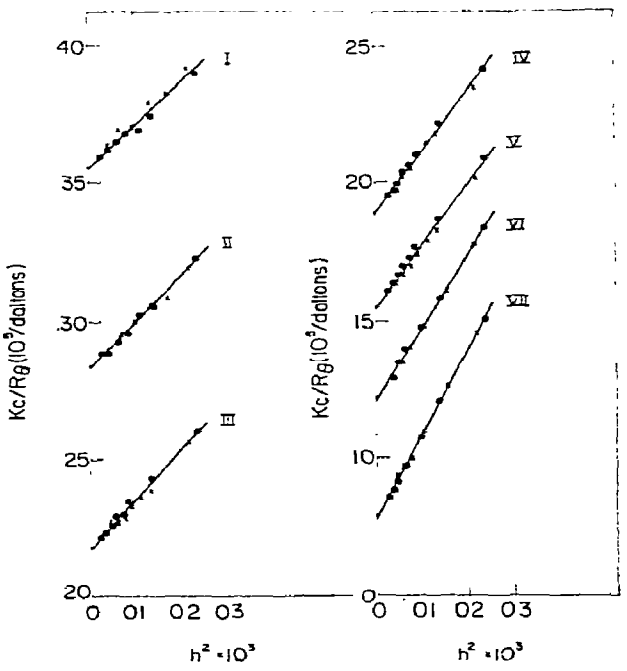

Fig. 4. Angular dependent extrapolations (at zero concentration) for Fractions I–VII. (×) at 436 nm; (•) at 546 nm. Extrapolations are by least squares fit. (The $\theta = 60^{\circ}$ data point for each fraction at 546 nm is included, although it was not included in the extrapolation procedure.) Measurements at 25°C.

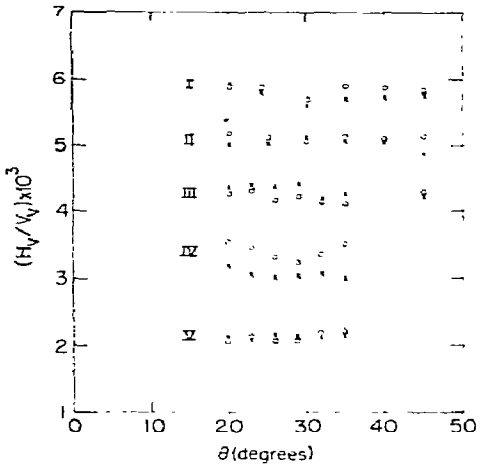

Fig. 5. Depolarization ratios under conditions of vertically polarized incident light (ρ_v) as a function of scattering angle for fractions I–V. (○) at 546 nm; (×) at 436 nm. Measurements at 25°C.

4.2. Optical anisotropy corrections

Scattering intensity measurements under polarization conditions of H_v were made on the highest concentration samples of Fractions I–V[‡] at several angles between $\theta_{20}°$ and $\theta_{45}°$. Values of ρ_v (i.e., H_v/V_v; the V_v intensities were from the measurements described above) are plotted as a function of θ in fig. 5. No angular dependence common to the five sets of values was evident; therefore, the average value of a particular set was assumed to closely approximate $(\rho_v)_{\theta=0}$ for that fraction. From the values of $(\rho_v)_{\theta=0}$, anisotropy ratios (δ) were calculated (eq. (6)) and these in turn used in eqs. (3) and (4) to obtain corrected values for the weight average molecular weights and Z-average mean square radii (table 1). Because anisotropy ratios could not be calculated for Fractions VI and VII, the molecular weights and mean square radii of these fractions were corrected using the value for δ determined for Fraction V (see below). The error limits included with the corrected molecular weights are the standard errors of estimate from the least squares extrapolations of the zero angle plots (fig. 3). The limits on the mean square radii are proportional to the standard errors for estimate obtained from the least squares extrapolations of the angular dependence plots (fig. 4); i.e., the error value in each case was multiplied by R_{gz}^2/M_w^{-1}.

The corrections applied to the molecular weights were all within the limits of the experimental errors for the molecular weight determinations, the highest (Fraction I) being less than 1%; the corrections to the mean square radii, however, were significant, ranging from 4 to 7%. Since δ was found to vary inversely with fragment length (see fig. 6), the corrections applied to Fractions VI and VII are undoubtedly too large. But as will be seen below, the anisotropy corrections have only minor effect on the calculated persistence lengths of the two highest molecular weight fractions.

[‡] Fractions VI and VII were also measured (prior to Fractions I–V), but the intensities were falsely high due to improperly aligned polarizers.

Table 1
Light scattering molecular weights, mean square radii, and optical anisotropy ratios [a]

Fraction	Weight average molecular weight ($\times 10^{-5}$)		Z-average mean square radius ($\times 10^{-2}$ nm^2)		Root mean square radius (nm)	Anisotropy ratio
	M_w^* [b]	M_w [c]	R_{gz}^{2*} [b]	R_{gz}^2 [d]	R_{gz}	δ [e]
I	2.84	2.82 ± 0.03	12.89	12.00 ± 0.19	34.6	− 0.096
II	3.58	3.56 ± 0.03	17.89	16.71 ± 0.25	40.9	− 0.091
III	4.66	4.63 ± 0.04	25.18	23.68 ± 0.21	48.7	− 0.082
IV	5.32	5.29 ± 0.05	35.75	33.84 ± 0.64	58.2	− 0.072
V	6.51	6.49 ± 0.06	43.17	41.31 ± 0.81	64.3	− 0.058
VI	8.29	8.26 ± 0.04	64.26	61.48 ± 0.84	78.4	– g)
VII	12.73	12.69 ± 0.04	115.99	110.99 ± 1.53	105.3	– g)
VII (5°C)	12.73 [f]	12.69 ± 0.04 [f]	113.90	108.99 ± 2.95	104.4	– g)
VII (45°C)	12.73 [f]	12.69 ± 0.04 [f]	102.42	98.01 ± 2.03	99.0	– g)

a) Measurements at 25°C, unless otherwise indicated.
b) Average of apparent values at 436 and 546 nm incident light.
c) Apparent values corrected for optical anisotropy; limits are standard errors of estimate of the least squares extrapolations (fig. 3).
d) Apparent values corrected for optical anisotropy; limits are proportional to the standard errors of estimate of the least squares extrapolations of the infinite dilution extrapolates (fig. 4); also see text.
e) Average of the values at 436 and 546 nm incident light.
f) Value measured at 25°C assumed.
g) Not measured (see text).

Table 2
Weight and Z-average fragment contour lengths and persistence lengths from light scattering measurements [a]

Fraction	Weight and Z-average contour length (nm) and ratio			Persistence length, a (nm)	
	L_w [b]	L_z [c]	L_z/L_w [d]	a^* [e]	a [f]
I	144	154	1.07	64.1	52.2
II	186	199	1.07	51.9	45.8
III	239	249	1.04	53.3	48.0
IV	277	291	1.05	65.3	59.6
V	337	351	1.04	59.2	54.9
VI	434	469	1.08	58.9	55.3
VII	651	723	1.11	62.6	59.3
VII (5°C)	651 [g]	723	1.11	–	58.2
VII (45°C)	651 [g]	723	1.11	–	51.4

a) Measurements at 25°C, unless otherwise indicated.
b) Average of values from light scattering and sedimentation equilibrium (accompanying paper [1]) assuming 1950 daltons/nm for the sodium salt of double-stranded DNA.
c) Calculated from Z-to-weight average contour length ratios (next column).
d) From electron micrograph histograms (fig. 8, accompanying paper [1]).
e) Calculated from mean square radii uncorrected for optical anisotropy (table 1, column 4).
f) Corrected for optical anisotropy.
g) Value measured at 25°C assumed.

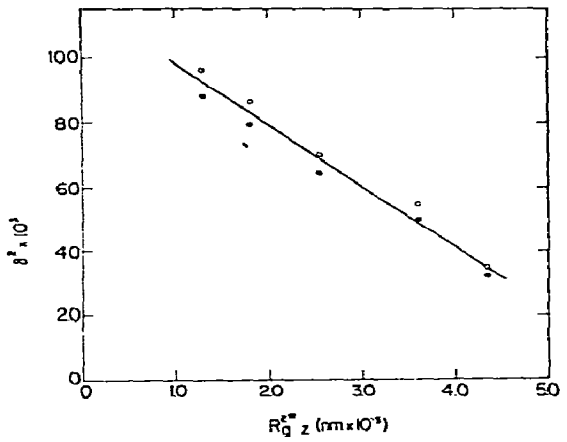

Fig. 6. Optical anisotropy ratios, squared (δ^2), plotted as a function of apparent mean square radii for fractions I–V. (○) at 436 nm; (●) at 546 nm.

4.3. Temperature studies

The mean square radii for Fraction VII at 5 and 45°C (table 1) were calculated from eq. (2) assuming M_w^* to be equal to the value obtained at 25°C. This procedure precluded evaluation of the several constants contained in K and ΔR at the higher and lower temperatures. Only the solvent refractive index, which appears in h^2, required re-evaluation; it was assumed that n_0 has the same temperature dependence as water. It was further assumed that the anisotropy correction determined at 25°C also applied at the other two temperatures.

4.4. Estimation of persistence lengths from light scattering

The weight average molecular weight of each fraction was taken to be the average of the values obtained from light scattering and the sedimentation equilibrium measurements (except in the case of Fraction VII which was not measured by sedimentation equilibrium). Assuming that the fragments conformed to the B structure [18,19] for double-stranded DNA, with a mass per unit length of 1950 daltons/nm, these values were converted to weight average contour lengths (table 2). The 640 or more measured particle lengths comprising each histogram (fig. 8, first paper [1]) were then corrected to new values by a factor which equated the weight average length of the histogram with the experimentally determined weight average contour length of the corresponding fraction. By assuming a value for the persistence length, mean square radii were generated (eq. (8)) with the aid of a computer for all the corrected contour lengths contained in each histogram. Each generated mean square radius was corrected for the effects of optical anisotropy by eq. (4) using a value for δ determined by an empirical linear function relating δ^2 to R_{gz}^{2*} (fig. 6):

$$\delta^2 = 1.17 \times 10^2 - 1.19\, R_{gz}^{2*} \times 10^{-6}.$$

δ^2, however, was not allowed to be less than 0.003 – a value slightly lower than that measured for Fraction V – for the purposes of this correction procedure.

The Z-average was then calculated for the 640 or more corrected mean square radii from:

$$R_{gz}^2 = \sum R_{gi}^2\, Ni\, L_i^2 / \sum Ni\, L_i^2.$$

This process was repeated for several values of a at 5 nm intervals chosen to generate mean square radii which would encompass the experimentally determined value for the particular fraction. The persistence length was then calculated by linear interpolation.

The persistence lengths for the seven fractions are listed in table 2; also included are the values which are obtained when optical anisotropy corrections are not applied. It is evident that a is not length dependent, at least within the molecular weight range of the DNA fractions examined. This is more easily seen in fig. 7 where both the persistence lengths (corrected and uncorrected) and the mean radii (R_{gz}) are plotted as a function of the Z-average contour length. These last values were obtained from the weight average lengths and the Z-to-weight average ratios calculated from the contour length histograms (fig. 8, accompanying paper [1]). Also seen in the figure are the values for a and R_{gz} determined for Fraction VII at 45°C.

4.5. Sedimentation and viscosity:

For the evaluation of the persistence length from the sedimentation results we correct $\phi'\rho$ (equal to $1-(\partial\rho/\partial c)_\mu$ [15]), determined [1] to be 0.550 in solvent B at 25°C,

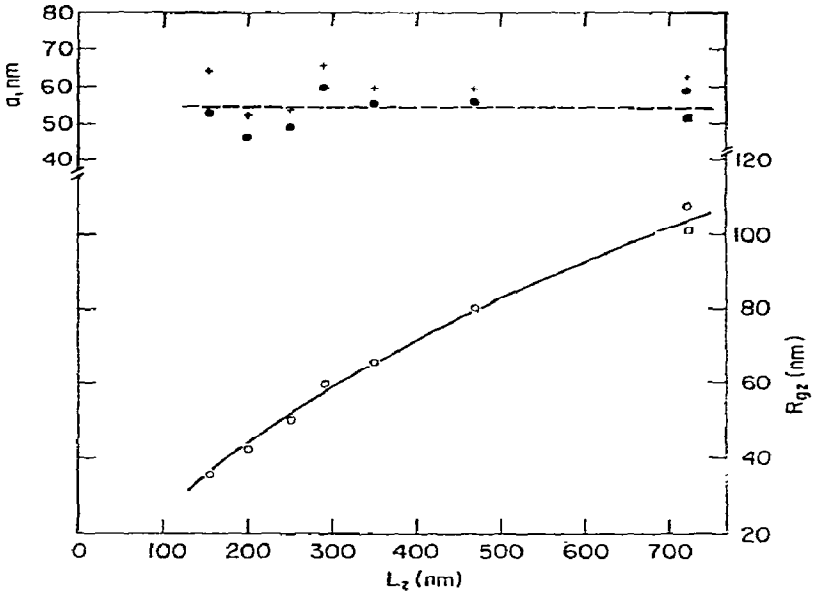

Fig. 7. Persistence lengths and mean radii (R_{gz}) as a function of Z-average contour length. (•) Persistence lengths corrected for optical anisotropy; (+) uncorrected persistence lengths. (▪) corrected persistence length for Fraction VII measured at 45°C. (□) R_{gz} for Fraction VII measured at 45°C. Other values measured at 25°C.

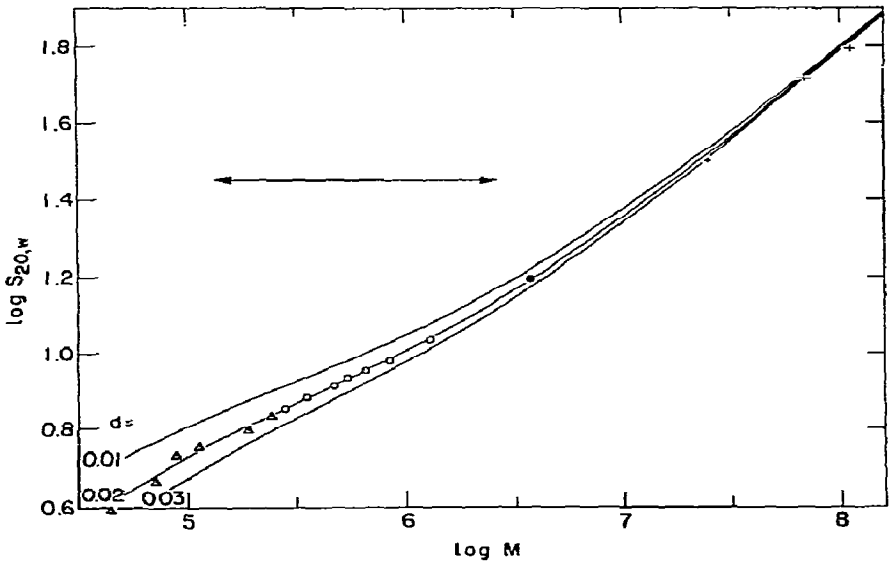

Fig. 8. Log $s_{20,w}$ versus log M curves, calculated according to Yamakawa and Fujii [7,8]; d is the reduced thickness parameter; M_L = 1950 daltons/nm. (Δ) Record et al. [21]; (○) Ref. [1]; (•) Jolly and Eisenberg [22]; (+) Schmid et al. [3]. The calculated curves (log s versus log L + log M_L) are horizontally displaced (cf. double arrow in figure) by log λ^{-1} = 2.12. The corresponding value for λ^{-1} is 132 nm and the persistence length, $a = 1/2\lambda$, equals 66 nm. The unreduced thickness is 0.02 × 132 = 2.64 nm. cf. eqs. (13) and (11a).

to 0.546 in water at 20°C. We substitute the value for $\phi'\rho$ in eq. (13), and with 0.01 P for η_0 (water at 20°C), 1950 nm for M_L, we find

$$\log s_{20,w} = 0.4583 + \tfrac{1}{3}\Gamma_2 + \tfrac{1}{2}\log L; \qquad (19)$$

Using the extensive tables for $\Gamma_2(L,d)$ provided by Yamakawa and Fujii, we plot calculated values of $\log s$ according to eq. (19) against $\log M_L L$ for various values of d (fig. 8). The experimental results are plotted as $\log s_{20,w}$ against $\log M_w$. The best overlap between the calculated curves and the experimental points achieved by a horizontal shift (arrow in fig. 8) defines $\log \lambda$:

$$\log (M_L L) - \log M = -\log \lambda, \qquad (11a)$$

which corresponds to the value of the persistence length for an appropriate value of d. As M_L is accurately known for the B form of Na-DNA, it has been fixed and not left as an adjustable parameter as in the procedure recommended by Yamakawa and Fujii.

The sedimentation velocity curve (fig. 8) agrees with experimental results from several sources over almost a 10^4 range in molecular weight, with a reasonable value for the chain thickness, $d = 0.02$*. The values from the companion study [1] span the intermediate range of molecular weights, between 0.28 to 1.3×10^6 daltons; values of s in the lower molecular weight range (down to 4.5×10^4) have been taken from the work of Record et al. [21] who carefully characterized fractionated DNA fragments of this size. The point at $M_w = 3.75 \times 10^6$ is a sheared and fractionated sample of calf thymus DNA of Jolly and Eisenberg [22]. For all these fractions we have used the weight average value of the molecular weight in conjunction with the weight average value of s. In view of the fact that the distribution of all the fractions, as characterized by electron microscopy, is rather narrow (M_w/M_n is between 1.04 and 1.10) this procedure presently appears justified. The three high-molecular weight points are homogeneous DNA preparations from the coliphages T7, T5, and T4. In spite of extremely careful molecular weight determinations, by use of a variety of methods, an uncertainty of about ±5% remains in their molecular weights [3]. Molecular weights and sedimentation coefficients have been reported for DNA's from other sources as well (including even higher molecular weight bacterial DNA's), but none of these results match the reliability of the information extant with respect to the coliphage samples. From the shift required to bring the calculated and experimental curves into coincidence (fig. 8), we find $\log \lambda^{-1} = 2.12$, which corresponds to $\lambda^{-1} = 131.8$ nm, and a Kratky–Porod persistence length, a, equal to about 66 nm for a chain diameter of about 2.6 nm. As pointed out by Yamakawa and Fujii, the last quantity is not obtained with any degree of accuracy from the theoretical analysis.‡

For the evaluation of the persistence length from the viscosity data a plot of the theoretical values for $-\frac{2}{3}\Gamma_1$ (eq. 16) against $\log M_L L$ is shifted by equal numerical displacement of the abscissa and ordinate (cf. arrow in fig. 9) with respect to a plot of the experimental quantities (left-hand side of eq. (16)) versus $\log M$. As before (cf. eq. (11a)) the shift equals $\log \lambda^{-1}$, in this case along both axes.

The low molecular weight results in fig. 9 derive from the companion work [1]. The point at 3.75×10^6 daltons is from Jolly and Eisenberg [22]; and the phage data is summarized from Hearst et al. [23] and Schmid et al. [3]. An additional viscosity value for T7 double stranded DNA is due to Rosenberg and Studier [24] — 119 dl/g versus 111 dl/g of Hearst et al. [23]. Unfortunately, no viscosities were measured of the very low molecular weight samples studied by Record et al. [21], so the molecular weight range is more restricted than in the case of the sedimentation analysis. The molecular weight corresponding to the intrinsic viscosity is the so-called viscosity average molecular weight, M_v [25], rather than the weight average molecular weight, M_w, used here for the fractionated calf thymus DNA samples.

* The reader who would like to convince himself that other values of d do not yield a satisfactory fit should place a transparent sheet over fig. 8 and mark the experimental points and the coordinates. Overlap [upon a horizontal shift, as explained with respect to eqs. (13) and (11a)] with either $d = 0.01$ and 0.03 is not possible, even within the more restricted experimental range of our own data.

‡ The calculated curves of fig. 8 show that whereas in the high molecular weight range it is indeed impossible to discriminate between various chain thicknesses — as is intuitively reasonable — the data in the low molecular weight range allow more sensitive testing of the limits of the theoretical treatment with respect to this parameter.

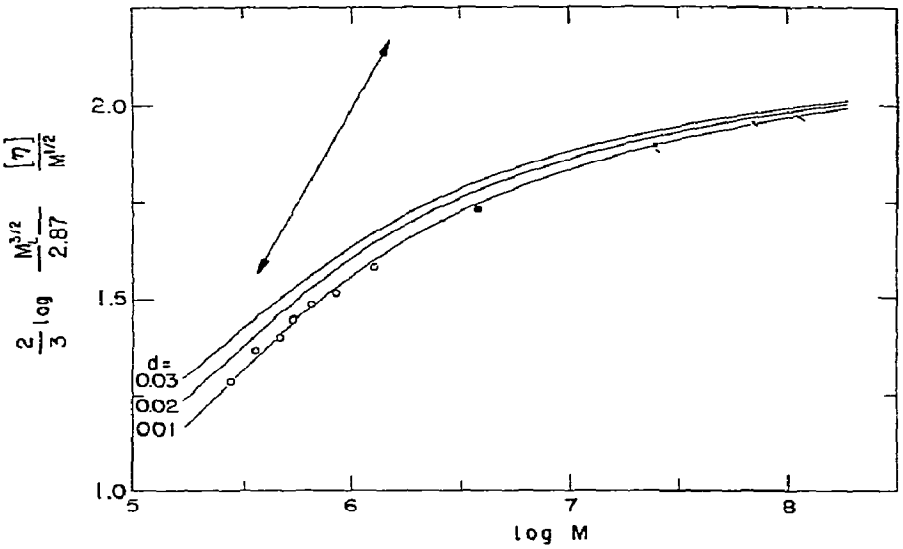

Fig. 9. The parameter $\frac{2}{3}\log\{(M_L^{3/2}/2.87)\,[\eta]/M^{1/2}\}$ versus $\log M$. Curves, calculated according to Yamakawa and Fujii [8]; d is the reduced thickness parameter; M_L = 1950 dalton/nm. (○) Ref. [1]; (●) Jolly and Eisenberg [22]; (△) Hearst et al. [23] and Schmid et al. [3]; (×) Rosenberg and Studier [24]. The calculated curves are displaced equally along abscissa and ordinate (cf. double arrow in figure) by $\log \lambda^{-1}$ = 2.07. The corresponding value for λ^{-1} is 118 nm and the persistence length, a $(1/2\lambda)$, equals 59 nm. The unreduced thickness is 0.01 × 118 = 1.18 ≈ 1.2 nm. (cf. eqs. (16) and (11a)).

The value of M_v is sufficiently close to M_w that, for the narrow fractions examined here, the use of M_w does not lead to significant error.* Although the value of $\log \lambda^{-1}$ is rather insensitive to the exact value of d, the curve for $d = 0.02$ is not fitted well (place transparent sheet over fig. 9, mark experimental points and arrow, and shift along arrows). The best fit is found for $d = 0.01$, and we find $\log \lambda^{-1} = 2.07$, corresponding to λ^{-1} equal to 117.5 nm, a persistence length of about 59 nm, with an unreduced thickness of 1.2 nm. This value for d is rather low; the thickness of the high humidity B form of the DNA chain determined by X-ray diffraction and scattering is about 2.4 nm (cf. Bloomfield et al. [4], p. 199 l.c.). In fig. 10 we have plotted $\log [\eta]$ against $\log M_w$; the parameters M_L = 1950 nm, λ^{-1} = 117.5 nm, and $d = 0.01$, define the curve from the theory of Yamakawa and Fujii.

* The viscosity average molecular weight M_v equals M_w, if a_η, defined by $[\eta] \propto M^{a_\eta}$, is equal to unity (Flory [25], page 312)). We estimate (fig. 10) $a_\eta \approx 1.25$ in the range $0.3 < M_w \times 10^{-6} < 1.3$ and $a_\eta \approx 1.1$ in the range $1.3 < M_w \times 10^{-6} < 3.75$, and believe M_v to be rather close to M_w for our narrowly distributed fractions ($1.04 < M_w/M_n < 1.10$).

Finally, we calculate the Flory–Mandelkern parameter, β, from theory over the range of molecular weights for comparison with experimental results (fig. 11). For this enterprise we have calculated $\beta(L, d)$ by eq. (18) and shifted these values to the molecular weight scale by use of eq. (11a) with M_L = 1950 daltons/nm and $\log \lambda^{-1}$ = 2.08 (the exact value of $\log \lambda^{-1}$ used here is not important). The value of β has been calculated once using (a) $d = 0.02$ for both Γ_2 and Γ_1, and then (b) with $d = 0.02$ for Γ_2 and 0.01 for Γ_1. The experimental results are slightly lower than the calculated values, yet the same pattern of behavior is followed throughout.

5. Discussion

From the limiting dependence of scattering on scattering angle, we obtained by use of eqs. (1) and (2) the Z-average of the radius of gyration, R_g, after suitable corrections for optical anisotropy. From R_{gz} we obtained by eq. (8), and by procedures described in the text, a value for the persistence length a; proper account was

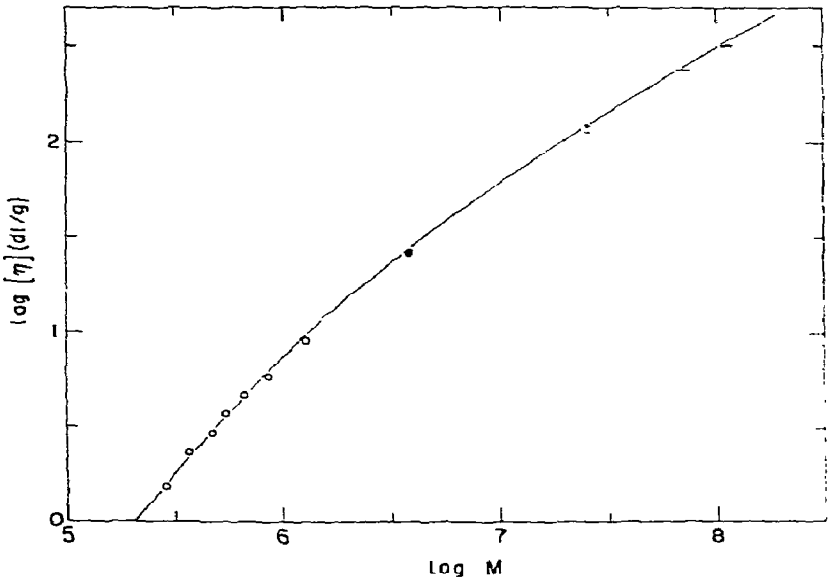

Fig. 10. Viscosity $[\eta]$ (dl/g) versus M. (○) ref. [1], (●) Jolly and Eisenberg [22]; (–) Hearst et al. [23] and Schmid et al. [3] (+) Rosenberg and Studier [24]. Curve calculated according to Yamakawa and Fujii [8] with M_L = 1950 daltons/nm, d = 0.01 and log λ^{-1} = 2.08.

taken of the known (from electron microscopy) limited polydispersity of the samples. The procedure for deriving R_{gz} for these samples is valid because, in the molecular weight range of our samples (0.3 to 1.3×10^6) and at low angles of scattering ($45° > \theta > 20°$), the extrapolation to zero value of h (fig. 4) fulfills the condition that $h^2 R_g^2$ be low enough (less than 0.5, for instance) for the lowest points to lie on the Zimm limiting curve [10]. Another condition fulfilled here is that excluded volume effects are absent in the molecular weight range examined. We use a condition established by Hays et al. [26]:

$$R_g^2/R_{g0}^2 = 1 + 0.0572\, A_2\, M^2/N_A\, R_{g0}^3\,, \qquad (20)$$

from which it follows that the ratio of R_g, perturbed by excluded volume effects, to R_{g0}, in the absence of such effects, is close to unity (about 1.03) for the highest molecular weight sample ($M_W = 1.27 \times 10^6$; $R_g = 1.05 \times 10^{-5}$cm).*

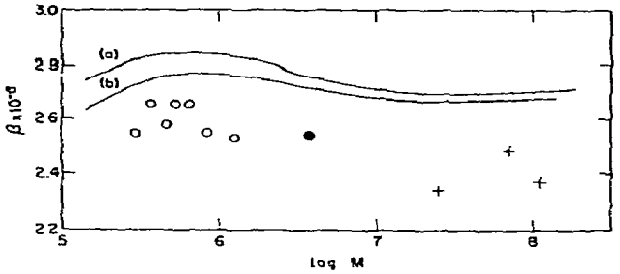

Fig. 11. Flory–Mandelkern parameter β versus M. Curves calculated according to Yamakawa and Fujii [7,8], cf. eqs. (17) and (18); M_L = 1950 dalton/nm. Curve (a), d = 0.02; curve (b), d = 0.02 for Γ_2 and 0.01 for Γ_1. (○) ref. [1], (●) Jolly and Eisenberg [22]; (+) Hearst et al. [23] and Schmid et al. [3].

In our studies we found values of A_2 (cf. table 2 of the preceding paper [1]) around 5×10^{-4} mole ml/g^2; Jolly and Eisenberg [22] report about 4×10^{-4} at $M_W \approx 3.75 \times 10^6$, Harpst et al. [28] find 3×10^{-4} for calf thymus DNA ($M_W \approx 18 \times 10^6$) and less defined

* From the Yamakawa–Stockmayer theory of the excluded volume effect in wormlike touched-bead models (27) it can be shown (H. Yamakawa, private communication) that the expansion factor is even closer to unity (less than 1.01) for our highest molecular weight sample.

values for T7 DNA. We can thus assume, for the purpose of this estimation, an average value of 4×10^{-4} for A_2 over a wide range of molecular weights at 25°C and in essentially 0.2 M NaCl solvent.

From the analysis of the limiting scattering curves we obtained (table 2) values for the persistence length with reasonable scatter, yet without a discernably significant trend (fig. 7). The average value of a is calculated to be 54.0 ± 5.6 nm. Jolly and Eisenberg [22] have reported a value of 66 ± 6 nm for a single sample of $M_w = 3.75 \times 10^6$ from laser light scattering analysis. These results when compared with acceptable values of a recently reviewed in the literature [4,29] clearly show that, within the relatively large error associated with this determination, a does not increase with decrease in M (at least down to 3×10^5 daltons). This finding therefore refutes the earlier preliminary suggestion (Cohen and Eisenberg [30], Eisenberg [31]) that a might increase considerably with decreasing chain length. Our present results, therefore, strongly indicate that (a) the flexibility of double-stranded DNA is independent of chain length at least in the low molecular weight range in which a gradual transition from the properties of a stiff coil to those of a flexible rod are likely to occur, and (b) the simple Kratky–Porod model adequately describes the DNA chain with a single flexibility parameter.

Additional support for the findings reported above come from the sedimentation and intrinsic viscosity measurements. Measurements of these hydrodynamic quantities are precise, yet their theoretical interpretation in terms of polymer chain conformation is not as straightforward as the analysis of the more difficult light scattering experiments. For a recent discussion of the limitations in the hydrodynamic treatments to date, we refer to the papers by Yamakawa and Fujii [7,8]. One may conclude that the parameter obtained with some reliability is the persistence length, whereas the thickness of the chain (which is orders of magnitudes lower than the contour length) cannot be obtained with any degree of confidence. The hydrodynamic translational and rotational friction resistences are therefore not sensitive to the molecular thickness parameter; this is clearly reflected in the theoretical analysis. Considerable variations in the thickness parameter, d (compare figs. 8 and 9), do not shift the theoretical curves for the sedimentation or the viscosity of chain-like molecules to a large extent.

The results for the sedimentation curves are particularly striking. Over a very wide range of molecular weights, from the lowest chain length samples of Record et al. [21], throughout the intermediary range, and into the high molecular weight range of the coliphage DNA's, the curves are extremely well fitted by a single persistence length ($a = 66$ nm) and a single chain diameter of 2.6 nm. The latter value is in agreement with the value derived for the diameter of duplex DNA from X-ray diffraction and scattering studies [4]. Yet a puzzling feature is in the agreement between experiment and theory at the high molecular weight end, in the absence of excluded volume corrections. From eq. (20) we concluded that at $M \approx 10^6$ excluded volume effects were negligible, yet at $M \approx 25 \times 10^6$ (T7 DNA) Hays et al. [28] estimate a correction in linear dimensions of about 10%, and for T4 DNA, in the molecular weight range around 10^8, linear dimensions of chains with excluded volume might be 20% to 25% higher than in the absence of this effect. The fact that the experimental results are described in terms of a unique persistence length, although excluded volume was not considered in the theoretical treatment, suggests that excluded volume effects may influence the sedimentation rate of DNA much less than currently believed (see also footnote, p. 15).

From the viscosity results we find (fig. 9) a persistence length of 59 nm but an unusually low value (~ 1.2 nm) for the thickness of the DNA chains ($d = 0.01$). We have already remarked that the chain thickness is not a parameter to be relied on in an analysis of the hydrodynamic data. If we shift the experimental data (following the procedure outlined in section 4) for a best fit of the low molecular weight points (open circles) with $d = 0.02$, we find that the fit of these points is not as good as before, the value at 3.75×10^6 (black circle) deviates upwards and high molecular weight phage data are considerably too high. The discrepancy might be due to the fact that, in contrast to sedimentation, viscosity is more sensitive to excluded volume chain expansion effects. The shift of the low molecular weight data (open circles) from $d = 0.01$ to $d = 0.02$ (along the arrow) moderately reduces a from 59 to 50 nm and raises the chain thickness to 2.0 nm. Some intermediate value between $d = 0.01$ and $d = 0.02$ could be chosen but no deeper physical insight is gained unless some more positive statement about the excluded volume effect in the high molecular weight range can be made. On the other hand, shifting of the high molecular phage data from $d = 0.01$ to $d = 0.02$

hardly affects the value of a and leaves the low molecular weight data on the curve for $d = 0.01$. This is due to the fact that in the high molecular weight range the curves for the various values of d converge, and it is virtually impossible to derive a value for this parameter from experiment.

In conclusion we can calculate an average value of a from the three methods described: For light scattering we include the value (66 nm) of Jolly and Eisenberg [22] as a single value point, which raises a from 54 to 55 nm; from sedimentation and viscosity we obtained 59 and 66 nm respectively. The average value of a is 60 ± 6 nm which we believe to be a satisfactory value of a over the molecular weight range in which reliable experimental data are available.

If we take $a = 50$ nm from the viscosity results by shifting the low molecular weight data to $d \approx 0.02$ (see above), then the average value of a from the three sets of experiments only drops to 57 ± 8 nm.

From the Yamakawa and Fujii treatment, we have plotted the Flory–Mandelkern parameter, β (eq. 18)), against h in fig. 11. The experimental values (cf. eq. (17)) are slightly lower, but follow a similar trend. Fig. 11 represents an interesting demonstration of the extent to which hydrodynamic data can be compared with theoretical estimates, using the barest minimum of adjustable parameters.

The temperature dependence of R_g has been measured for Fraction VII. We did not observe a change in persistence length at 5°C when compared with 25°C, yet at 45°C a was found to be significantly lower (cf. table 2). The number of temperature points measured is not sufficient for a quantitative evaluation of the temperature effect. Gray and Hearst [32] also found (from sedimentation velocity studies) that a decreases with increasing temperature, and Cohen and Eisenberg [30] had made similar observations from viscosity studies. From an accurate knowledge of the temperature dependence of a it is possible [32] to estimate the entropy and enthalpy of bending of DNA chains, which are related to the problem of folding of DNA into compact biological structures. The persistence length a can be reformulated [33] in terms of a flexural rigidity parameter,

$$\epsilon = kTa, \qquad (21)$$

which we calculate to be (for $a = 60$ nm) equal to 2.5×10^{-19} dyn cm^2 at 25°C. This is twice as high as that reported by Sugi et al. [34] who had used a lower value of a.* Folding of the DNA chains into compact structures with these rigidity and thermodynamic parameters is plausible, even if the double helical structure is preserved (32,34).

Acknowledgment

The authors wish to thank Dori Cwikel for her expert technical assistance and computer analysis of the light scattering data. They also thank Dr. H. Yamakawa of Kyoto University for graciously furnishing numerical tables which aided in the estimation of the persistence lengths by the hydrodynamic theories for stiff coils of Dr. M. Fujii and himself.

References

[1] J.E. Godfrey, Biophys. Chem. 5 (1976) 285.
[2] O. Kratky and G. Porod, Rec. Trav. Chim. 68 (1949) 1106.
[3] C.W. Schmid, F.H. Rinehart and J.E. Hearst, Biopolymers 10 (1971) 883.
[4] V.A. Bloomfield, D.M. Crothers and I. Tinoco, Physical Chemistry of Nucleic Acids (Harper and Row, New York, 1974) ch. 5.
[5] P. Horn, Ann. Phys. 10 (1955) 386.
[6] G. Weill, C. Hornick and S. Stoylov, J. Chim. Phys. 64 (1968) 12.
[7] H. Yamakawa and M. Fujii, Macromolecules 6 (1973) 407.
[8] H. Yamakawa and M. Fujii, Macromolecules 7 (1974) 128.
[9] J.E. Hearst and W. Stockmayer, J. Chem. Phys. 37 (1962) 1425.
[10] H. Eisenberg, in: Procedures in Nucleic Acids, Vol. 2, eds. G.H. Cantoni and D.R. Davies, (Harper and Row, New York, 1971) p. 137.
[11] G. Cohen and H. Eisenberg, J. Chem. Phys. 43 (1965) 3881.
[12] D.J. Coumou, J. Colloid Sci. 15 (1960) 408.

* The numerical result is identical with the value reported by Cohen and Eisenberg [30], who calculated Youngs modulus to be 0.5×10^{10} dyn/cm^2 for a chain with assumed radius, r, equal to 0.9 nm, and moment of inertia of the cross section $I = \pi r^4/4$, ($\epsilon = EI$). The agreement is fortuitous as Cohen and Eisenberg [30] used a circular arc model (for $M_w \approx 5 \times 10^5$) for their DNA sample rather than the wormlike coil for which a substantially higher value of a (and therefore of ϵ) may be derived from the same data [31].

[13] D.J. Coumou, E.L. Marker and J. Hijmans, Trans, Faraday Soc. 60 (1964) 1539.
[14] C.H. Chervenka, A Manual of Methods for the Analytical Ultracentrifuge, (Beckman Instruments, Inc., Palo Alto, California, 1973) p. 69.
[15] E.F. Casassa and H. Eisenberg, Advan. Prot. Chem. 19 (1964) 287.
[16] R.S. Krishnan, Proc. Natl. Acad. Sci., India, Sect. A1 (1935) 782.
[17] M. Benoit and P. Doty, J. Phys. Chem. 57 (1953) 958.
[18] J.D. Watson and F.H.C. Crick, Nature 171 (1953) 737.
[19] M.H.F. Wilkins, J. Chim. Phys. 58 (1961) 891.
[20] B.H. Zimm, J. Chem. Phys. 16 (1948) 1093, 1099.
[21] M.J. Record, Jr., C.P. Woodbury and R.B. Inman, Biopolymers 14 (1975) 393.
[22] D. Jolly and H. Eisenberg, Biopolymers 15 (1976) 61.
[23] J.E. Hearst, C.W. Schmid and F.P. Rinehart, Macromolecules 1 (1968) 491.
[24] A.H. Rosenberg and F.W. Studier, Biopolymers 7 (1969) 765.
[25] P.J. Flory, Principles of Polymer Chemistry (Cornell University Press, Ithaca, New York, 1953).
[26] J.B. Hays, M.E. Magar and B.H. Zimm, Biopolymers 8 (1969) 531.
[27] H. Yamakawa and W.H. Stockmayer, J. Chem. Phys. 57 (1972) 2843.
[28] J. Harpst, H. Krasna and B.H. Zimm, Biopolymers 6 (1968) 595.
[29] H. Eisenberg, Hydrodynamic and Thermodynamic Studies, in: Basic Principles in Nucleic Acid Chemistry, ed. P.O.P. Ts'o (Academic Press, New York, 1974) p. 171.
[30] G. Cohen and H. Eisenberg, Biopolymers 4 (1966) 429.
[31] H. Eisenberg, Biopolymers 8 (1969) 545.
[32] H.B. Gray, Jr. and J.E. Hearst, J. Mol. Biol. 35 (1968) 111.
[33] L. Landau and E. Lifshitz, Statistical Physics (Pergamon Press, London, 1958) pp. 478–82.
[34] M. Sugi, M. Fuke and A. Wada, Polymer J. 1 (1970) 457.